Cooperativity between the Two Heads of Rabbit Skeletal Muscle Heavy Meromyosin in Binding to Actin

Paul B. Conibear* and Michael A. Geeves#

*Department of Biochemistry, University of Leicester, Leicester LE1 7RH, United Kingdom, and #Max-Planck Institut fur Molekulare Physiologie, Rheinlanddamm 201, 44026 Dortmund, Germany

ABSTRACT An extensive series of experiments in this laboratory has shown that the binding of actin to rabbit skeletal muscle myosin subfragment-1 (a single-headed subfragment) can be described by a two-step model, with formation of a weakly bound complex, the A-state, followed by an isomerization to a more tightly bound complex, the R-state. In this paper, we report on additional experiments comparing the subfragment-1 with heavy meromyosin (a two-headed subfragment). Using a modeling approach, we have quantitated the two-step binding for each of the two heads. This indicates that the binding is cooperative and leads to a more complex view of the acto-myosin interaction than has previously been acknowledged. Implications for the dynamic behavior of the two heads during muscle contraction are discussed.

INTRODUCTION

Muscle contraction is the result of an ATP-driven interaction of the two-headed motor protein myosin with actin (Cooke, 1986; Geeves, 1991). Although it is known that a single myosin head constitutes the minimal functional unit, the question of cooperativity between the two heads remains open (Bagshaw, 1987). In an attempt to address this question, we have carried out a series of solution experiments comparing myosin subfragment-1 (S1) with heavy meromyosin (HMM) with respect to their interaction with actin and with nucleotides and have analyzed the data using a modeling approach.

There is reasonable experimental evidence that, in the absence of actin, the two heads are independent with respect to the mechanism of ATP hydrolysis (Taylor, 1979). However, it is likely from a structural viewpoint that they are cooperative in binding to adjacent subunits on an actin filament (Hill and Eisenberg, 1980). On the one hand, the binding of one head might render the second head better oriented with respect to an adjacent subunit, so favoring its binding. On the other hand, it is likely that myosin undergoes steric strain when two heads that are joined at the neck region bind to adjacent subunits with the same orientation, and this would disfavor the binding of the second head (Offer and Elliott, 1978).

In an attempt to evaluate the overall balance between the opposed effects of orientation and steric strain, Goody and Holmes (1983) proposed a model represented by the following scheme:

$$(\mathrm{Ac})_2 + \mathrm{HMM} \overset{4K_S}{\rightleftharpoons} \underset{\text{one head bound}}{\mathrm{A_2{\cdot}HMM}} \overset{K_SC/2}{\rightleftharpoons} \underset{\text{both heads bound}}{\mathrm{A_2{:}HMM}} \quad (1)$$

In this model, $(\mathrm{Ac})_2$ is an arbitrary unit consisting of two adjacent actin subunits, K_S is the acto-S1 binding constant, and C is the effective concentration of the second head (the concentration of S1 required to bind to the same degree) and is a constant reflecting structural features of the system. The factors of 4 and 1/2 are statistical terms. This assignment of equilibrium constants assumes that each of the two heads have the same capacity to bind to actin as S1 but allows for cooperativity arising from structural factors of the kind discussed above. The degree of cooperativity is specified by the value of C. On this model, the acto-S1 and acto-HMM binding constants are related by

$$K_H = 2K_S(2 + K_SC), \quad (2)$$

where K_H (the acto-HMM binding constant) is defined as

$$K_H = \frac{[(\mathrm{Ac})_2 \cdot \mathrm{HMM}] + [(\mathrm{Ac})_2{:}\mathrm{HMM}]}{[(\mathrm{Ac})_2][\mathrm{HMM}]} \quad (3)$$

The Goody and Holmes model can account for the best available measurements, which suggest that, in the absence of nucleotide, both heads are bound ($K_S = 5 \times 10^6\ \mathrm{M}^{-1}$, $K_H = 4.6 \times 10^9\ \mathrm{M}^{-1}$; Greene and Eisenberg, 1980), whereas, in the presence of AMP·PNP, only one of the two heads binds at a time ($K_S = 8.3 \times 10^4\ \mathrm{M}^{-1}$, $K_H = 5.2 \times 10^4\ \mathrm{M}^{-1}$; Greene, 1981). These values suggest that $C = 90\ \mu\mathrm{M}$, which is similar to the local concentration of the tethered head, estimated on a geometrical basis as approximately 100 μM (assuming that it undergoes restricted diffusion within a sphere of radius equal to its length of 20 nm). This close correspondence between these two estimates of C is consistent with little cooperativity between the heads. This may reflect a fortuitous balance between effects of orientation and of steric strain, although direct evidence for either of these effects has been lacking.

The 3G model

In 1984, Geeves et al. proposed a model for the actomyosin ATPase (the 3G model) in which myosin and actin interact

Received for publication 17 September 1997 and in final form 30 April 1998.

Address reprint requests to Dr. Paul B. Conibear, Department of Biochemistry, University of Leicester, Leicester LE1 7RH, UK. Tel.: 44-116-2523450; Fax: 44-116-2523369; E-mail: pbc1@le.ac.uk.

0006-3495/98/08/926/12 $2.00

as follows:

$$A + M{\cdot}N \overset{K_1}{\rightleftharpoons} \underset{\text{A-state}}{A\text{-}M{\cdot}N} \overset{K_2}{\rightleftharpoons} \underset{\text{R-state}}{A{\cdot}M{\cdot}N}, \quad (4)$$

where M is a single myosin head, A is an actin subunit, and N represents bound nucleotide. In this scheme, binding occurs initially to form a complex in which the proteins are weakly bound (the A-M·N or A-state), followed by an isomerization to a more strongly bound complex (the A·M·N or R-state) involving a substantial global conformational change either within the myosin head or in the actomyosin interface. It was also proposed that the A-to-R transition was coupled to the force-generating event of the cross-bridge cycle. The most fundamental feature of the 3G model is that the protein-protein interaction takes place via the same principle conformational states (i.e., the A- and R-states) both in the absence of nucleotide and for each of the possible nucleotide states of the ATPase cycle. It was proposed that bound nucleotide modulated the interaction simply via changes in K_1 and K_2 (although changes in K_2 were considered more likely). The 3G model does not consider interactions between the two heads of myosin.

Experiments using the single-headed fragment S1 have shown that the interaction can be described by the proposed two-step mechanism, i.e., via two globally distinct conformational states both in the absence of nucleotide and with a range of bound nucleotide ligands. Experimentally we find that K_2 is markedly dependent upon the nucleotide bound, varying from 200 in the absence of nucleotide (only the R-state is occupied) to >0.01 with ATP bound (only the A-state is occupied); with ADP bound, K_2 is of the order of 10 (so the A-state is significantly occupied although as a minor component), and with both ADP and Pi bound, it is thought to be close to unity (Geeves, 1991). Also, the A-to-R transition is found to lead to accelerated product release (Geeves, 1991). These features are compatible with a vectorial interconversion between A- and R-states during the ATPase cycle; i.e., changes in the nucleotide state drive the A-to-R transition, which in turn allows product release to take place so that the cycle can be repeated (Geeves, 1991). There is evidence emerging from a synthesis of structural and kinetic information that both the A-state and the R-state are stereospecific (Geeves and Conibear, 1995). There is kinetic evidence for a preceding collision complex too, which is probably nonstereospecific, but this is thought to be insignificantly occupied under most conditions and is not considered further in the present paper (Geeves and Conibear, 1995).

In the present work, we set out to characterize the binding to actin of the two-headed HMM in terms of a class of model based on that of Goody and Holmes but incorporating also the two-step binding of the 3G model. This would seem to provide an approach by which the orientation and strain effects might be resolved, in the case that the two effects operate differentially between the actin-binding step and the A-to-R transition.

A new model for the binding of HMM to actin

Fig. 1 *a* shows a general scheme for the acto-HMM interaction with each component head binding via the two-step mechanism of the 3G model (the two-letter notation defining the actin-binding states on the 3G model, i.e., A-state, R-state, or dissociated (D) for each of the two component heads in any given duplex state). In this (and subsequent) schemes, it is assumed that each of the two heads of HMM are inherently the same (i.e., in free HMM, the two heads are identical and independent of one another, although this need not be the case when bound to actin). In terms of global conformation, given duplex states are assumed to be independent of the bound nucleotide, in line with the 3G model. The apparent complexity of this present scheme arises largely because a priori each of the two heads could exist independently in each of the three states. The pattern of steric strain can be predicted from the following assumptions: 1) the binding is stereospecific for both A- and R-states; 2) the A-to-R transition involves a reorientation of the actomyosin interface or of domains within the head to produce a displacement of the base toward the barbed end of the filament (the working stroke); and 3) the working stroke is comparable to the intersubunit distance for the actin filament.

These features are incorporated into Fig. 1. In this representation, the amount of strain induced depends on whether the first head is in the A-state or the R-state and on whether the second head binds toward the pointed end or the barbed end of the actin filament. If the first head is in the A-state, then binding of the second head to give either AA-state will induce strain equivalent to the actin subunit repeat of 5 nm. However, if the first head isomerizes to the R-state, the head-tail junction is shifted, becoming more closely aligned with one of the adjacent actin subunits. In this case, the two adjacent actin subunits are not equivalent. The formation of RA (second head binding toward barbed end) will induce little strain whereas AR (second head binding toward pointed end) will require more strain than AA. The subsequent isomerization of RA to RR will induce further strain as the two heads need to separate at the head-tail junction again. The strain induced on this transition is similar to that induced on formation of AA. The exact amount of strain induced by making these transitions depends on the working stroke compared with the actin subunit repeat. These are thought to be of comparable magnitude (Molloy et al., 1995), but whatever the exact relationship, RA will generally be less strained than other states, and AR will be the most strained state.

The extent to which transitions are inhibited by strain will depend on the relative magnitude of the strain energy and the free energy for the unconstrained transition (i.e., for S1). The relatively weak binding into an A-state provides less energy with which to pay the strain cost than does binding in an R-state (so AA and AR are probably inhibited completely whereas RA $\longleftrightarrow$ RR is expected to take place but with a reduced equilibrium constant). We therefore propose

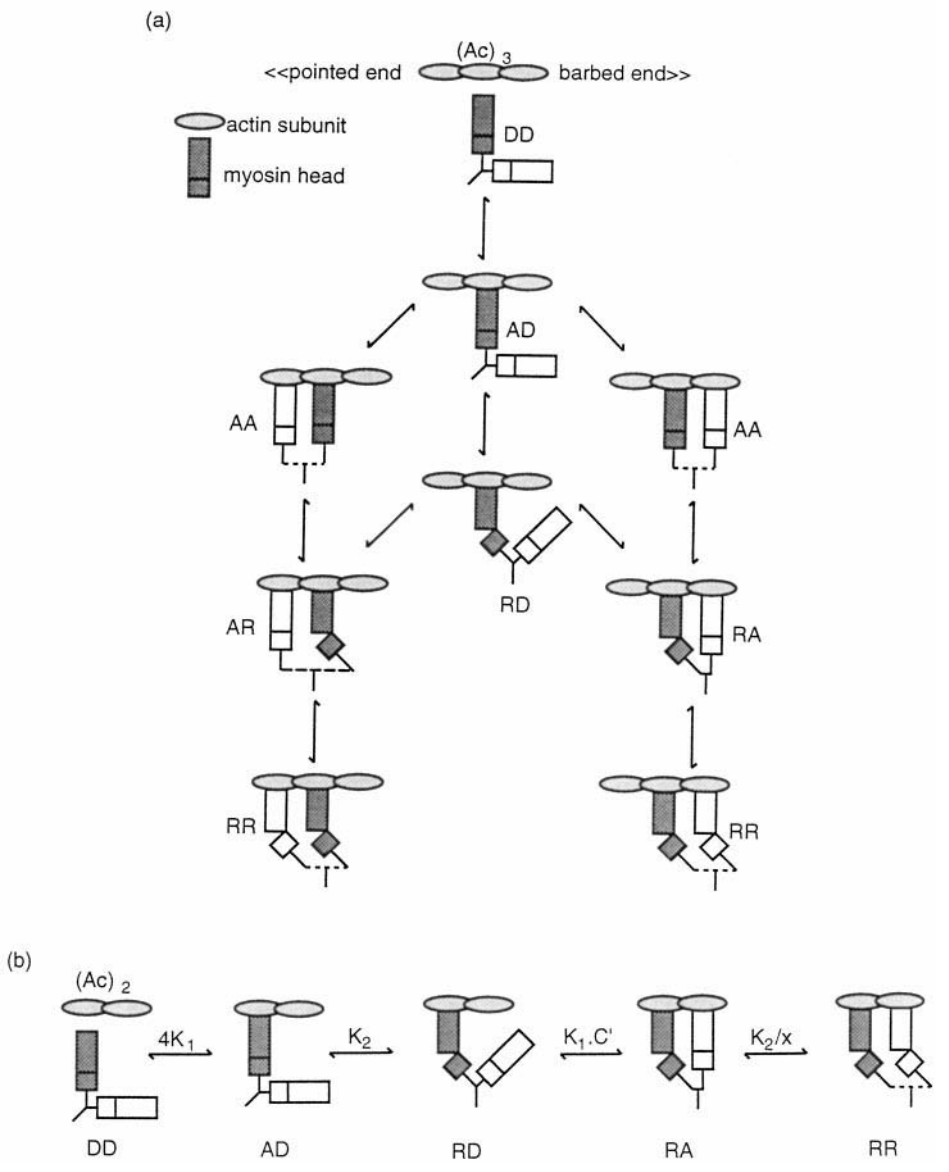

FIGURE 1 (*a*) General scheme for the acto-HMM interaction combining the features of Schemes 1 and 4. A two-letter notation is used to designate the actin-binding state of each of the two heads. Cartoon structures are shown for each state. The A-to-R transition is shown as involving an angle change in the domain distal to the actin-binding site, the so-called regulatory domain, in line with the nature of the force-generating event proposed by Rayment et al. (1993). In this representation, there is a state-specific strain in the neck region (the amount of strain is indicated by the dashed lines). The two heads of free HMM are assumed identical in this scheme, but they are distinguished by shading for clarity. (*b*) Proposed model for the acto-HMM interaction. This is based on *a* but with omission of the AA-states and the AR-state. Note the lack of strain in this model (except in the case of the RR-state).

a model in which the scheme of Fig. 1 *a* is reduced to the much simpler one of Fig. 1 *b*. In this model, the binding may be described as ordered and polar.

We have assigned equilibrium constants on our proposed model using the same principles as used by Goody and Holmes. The parameters K_1 and K_2 that appear here are the equilibrium constants that define the binding of S1 on the two-step binding model; C' is the effective concentration for the specified actin-binding step; x is the factor by which the equilibrium constant for the specified A-to-R transition is reduced relative to that for S1. The factor of 4 is a statistical term. C' and x are both constants reflecting the structural details of the system. Their precise values provide information on the degree and nature of the cooperativity, and as such, both of the latter steps can be modulated. On the basis of the pattern of distortion in the cartoon structures, we predict that C' is equal to or greater than 100 μM, the estimated local concentration of the tethered head, the precise value being determined by any orientation effect on this step; x is predicted to be greater than 1, the precise value being determined by the associated strain energy.

In this work, we have used methodology already established in our previous experiments with S1 but now applied to HMM in parallel experiments. Using equilibrium binding methods we have tested the proposed model (and alternative ones) and have calculated the parameters describing the cooperativity. The cooperativity is also examined at a dynamic level using stopped-flow methods.

MATERIALS AND METHODS

Proteins

S1 and HMM were prepared by chymotryptic digestion of rabbit skeletal muscle myosin based on the protocol of Margossian and Lowey (1982). Both subfragments were routinely purified either by ion exchange on DEAE-Sephacel or by ammonium sulfate precipitation, or both. Usually,

both proteins eluted as a single band, although occasionally, two equimolar fractions (corresponding to A1 and A2 isoforms) eluted separately, but they were pooled for use in subsequent experiments. For one experiment, HMM was further purified by an actin affinity centrifugation to remove ATP-resistant heads (Kron et al., 1991) followed by gel-filtration chromatography on a G-50 Sephadex spin column to remove the ATP required for the purification step. Column-purified HMM was contaminated with S1 to less than 5% by mass, and S1 was pure, as judged by SDS-polyacrylamide gel electrophoresis. F-actin was prepared by the method of Lehrer and Kerwar (1972) and labeled with pyrene as described previously (Criddle et al., 1985). Protein concentrations were determined by absorbance at 280 nm using $E^{1\%}$ values of 7.9 cm^{-1} (S1), 6.5 cm^{-1} (HMM), and 11.08 cm^{-1} (actin) with M_r values of 115 (S1), 360 (HMM), and 42 (actin). In assaying labeled actin, the pyrene absorbance was corrected for as described by Criddle et al. (1985).

Equilibrium binding measurements

These were carried out on a Perkin-Elmer LS-5B fluorimeter. Pyrene fluorescence was excited at 365 nm and emission monitored at 407 nm; 2.5-nm slit widths were used, except in experiments at low (0.1 μM) actin concentration where 5-nm slit widths were required for a satisfactory signal-to-noise ratio. Light scattering was measured in 90° mode with incident light of 411 nm, and the output monochromator was set at 413 nm (with 2.5-nm slit widths). For experiments where small optical amplitudes were measured, mechanical stabilization of the cell was required to maintain a stable signal.

Fluorescence titration data were analyzed by nonlinear least-squares fitting to

$$[A]_o\alpha^2 - \alpha([A]_o + [M]_o + 1/K) + [M]_o = 0, \qquad (5)$$

where $[M]_o$ is the subfragment concentration, K is the actin-binding constant (expressed per subfragment), and $[A]_o$ is the concentration of titratable binding sites. The latter parameter is allowed to float in titrations where the stoichiometry is to be determined (i.e., Fig. 2 *a*), but where K is to be measured (i.e., Fig. 2, *b* and *c*), it is set, in the S1 titrations, at the known value of the actin concentration or, in HMM titrations, at one-half this value (i.e., the concentration of the A_2 unit). α, the fractional association, is computed as

$$\alpha = (F_o - F)/(F_o - F_{max}), \qquad (6)$$

where F_o and F_{max} are the relative fluorescence intensities at zero and infinite concentrations of subfragment respectively. K, F_o, and F_{max} were generally allowed to float to optimize the fit.

Transient kinetics

Transients were measured using a Hi-Tech Scientific stopped-flow spectrophotometer (model SF-51) with illumination from a 100-W Hg-Xe arc lamp. The dead time was measured as ~1 ms. Drive movement occurs up to 1 ms after zero time but stabilizes thereafter. Pyrene fluorescence was excited at 365 nm and emission monitored through a KV393 glass filter (breakthrough of scattered light from the excitation beam was negligible). Light scattering was measured in 90° mode with incident light of 405 nm and without an emission filter. Signals from the photomultiplier were captured by an Infotech analog-to-digital converter using a Hewlett Packard 310 microcomputer. Data were analyzed either by least-squares fitting to exponential functions using software provided by Hewlett Packard run on the 310 computer or by simulation via numerical integration routines using the program KSIM run on an IBM personal computer (PS/2).

RESULTS

Evaluation of signals monitoring the interaction

A prerequisite for much of this work is the availability of signals that monitor the interaction with actin of each of the

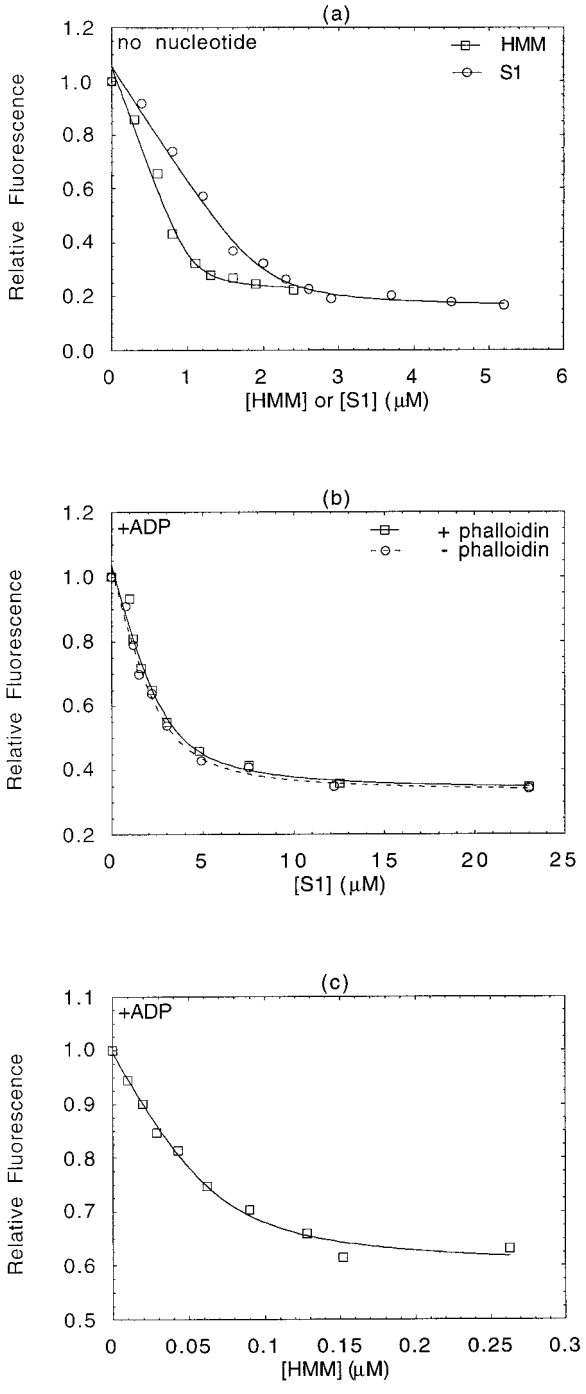

FIGURE 2 (*a*) Titrations were performed in the absence of nucleotide with 2 μM actin. The least-squares fit was obtained with $[A]_o$ = 2 μM and F_{max}/F_o = 15% for S1 and $[A]_o$ = 1 μM and F_{max}/F_o = 16% for HMM. (*b* and *c*) Titrations were performed in the presence of 2 mM ADP with actin concentrations of 1 μM (*b*) and 0.1 μM (*c*); 2 mM glucose and 20 μM hexokinase were added to the buffer before the experiment to remove contaminating ATP. The lines superimposed are the least-squares fits with fitted parameters as follows: $K_S = 5.7 \times 10^5$ M^{-1}, F_{max}/F_o = 22% (*b*, without phalloidin); $K_S = 6.7 \times 10^5$ M^{-1}, F_{max}/F_o = 25% (*b*, with phalloidin); $K_H = 3.3 \times 10^7$ M^{-1} and F_{max}/F_o = 53.5% (*c*). Duplicate experiments with the same subfragment preparations and phalloidin actin gave extreme values for K_S of 7.2×10^5 M^{-1} and 6.2×10^5 M^{-1} and K_H of 2.8×10^7 M^{-1} and 3.8×10^7 M^{-1} (n = 5). This is within the error calculated from residuals on fitting individual data sets. Buffer conditions: 0.1 M KCl, 5 mM $MgCl_2$, 20 mM MOPS, pH 7.0, at 20°C.

two heads of HMM independently and distinguish between the A-state and the R-state. For acto-S1, light scattering monitors the formation of any bound state (sum of both A- and R-states), whereas a fluorescent pyrene group covalently attached to actin at cys 374 provides a signal that monitors the formation of the R-state specifically (Coates et al., 1985; Criddle et al., 1985).

We have examined the fluorescence signal associated with the binding of the two heads of HMM by titration of both S1 and HMM against labeled actin in the absence of nucleotide (Fig. 2 *a*). This show a linear decrease in fluorescence with a sharp breakpoint. Direct fitting to the binding Eqs. 5 and 6 suggests there is one actin subunit per bound S1 compared with two per bound HMM. Both subfragments gave the same maximal quenching of fluorescence of 85%. Similar results have been reported previously (Criddle et al., 1985; Miyata et al., 1989). These data suggest that both heads bind to actin under these conditions, that they are both in the R-state, and that each results in an equivalent quenching of the fluorescence (as required).

Light-scattering signals are more complex and a priori could monitor the binding of only the first head (reflecting the increased mass of the decorated filament), or, on the other hand, a significant contribution could come from the binding of the second head, too (reflecting the reduced mobility of the bound head). We have tested this using the approach of Finlayson et al. (1969) but with the labeled actin. Here, the ATP-induced dissociation reactions of acto-HMM and acto-S1 were monitored by both fluorescence and light scattering in the stopped-flow spectrophotometer (Fig. 3). The fluorescence transients gave good fits to single exponentials (apart from brief push artifacts), and the observed rate constants vary linearly with ATP concentration, yielding second-order rate constants that are essentially the same in both cases ($2 \times 10^6\ M^{-1}\ s^{-1}$). Amplitudes are also the same for both proteins. This suggests that the two heads of HMM are independent and each identical to S1 for this process. This finding allows for a straightforward interpretation of the light-scattering transients. If both heads must dissociate for any change in light scattering to occur, then the light-scattering transient for HMM will lag behind that for S1, whereas if both sequential dissociation events contribute equally to the signal, the transients will be identical for both proteins (Taylor, 1979). Experimentally, a lag was not observed. Apart from brief push artifacts, both transients are well described by a single exponential, and the second-order rate constants are essentially the same for both subfragments ($2.4 \times 10^6\ M^{-1}\ s^{-1}$), indicating that to a good approximation light scattering also reports on each of the two heads.

Actin-binding constants

We have used the fluorescence titration method to measure the actin-binding constants of the two subfragments (i.e., K_S and K_H). This requires actin concentrations comparable to or lower than the inverse of the binding constant to be measured. Titrations in the absence of nucleotide such as those in Fig. 1 *a* do not allow an accurate measurement because the binding is too tight (Criddle et al., 1985; Kurzawa and Geeves, 1996). Thus, titrations were carried out in the presence of saturating ADP where the binding is weakened and at lower actin concentrations (Fig. 2, *b* and *c*). To prevent the actin from depolymerizing, which would otherwise occur at these lower concentrations (Kouyama and Mihashi, 1981), it was preincubated with phalloidin. That the actin was fully polymerized was confirmed by measuring the ratio of the emission intensities at 365 and 344 nm, as described by Kurzawa and Geeves (1996). Under these conditions, the titrations gave a nonlinear decrease in fluorescence. Nonlinear fitting yielded best-fit parameters of $K_S = 6.7 \times 10^5\ M^{-1}$, in agreement with the earlier work of Geeves (1989), and $K_H = 3.3 \times 10^7\ M^{-1}$. K_S can be measured at a supercritical concentration of actin and so can be measured in both the presence and absence of phalloidin. Such a comparison suggests that phalloidin has no major effect on the acto-S1 interaction.

The A-to-R equilibrium

We measured θ_S and θ_H (the fraction of bound actin subunits that are in the A-state in the presence of ligand) under the conditions of the titrations used for the experiment of Fig. 2, *b* and *c*, using a refinement of the method of Geeves and Jeffries (1988). This method provides a direct measure from the fluorescence change upon addition of ADP to the protein complex under nondissociating conditions (a fluorescence increase arising because the low-fluorescence A-state becomes significantly occupied after nucleotide binding) and is therefore applicable to both S1 and HMM. The results of such an experiment are shown in Fig. 4, *a* and *b*. The fluorescence increase is almost a factor of three smaller for S1 compared with HMM at 6.5% and 15.4% of the change for full dissociation, respectively, the latter being determined by subsequently adding ATP (the small ADP-induced changes are perhaps more clearly illustrated in Fig. 5). Essentially the same values were observed with a cell of smaller path length (2 mm compared with 1 cm) and when the signal was corrected for changes in the transmission of the excitation beam (which are immeasurable on addition of ADP). At lower concentrations of HMM, consistent results were obtained (differing only via dissociative contributions, assessed as discussed below). These control experiments all suggest that a differential inner filter effect is not contributing to the measured amplitudes.

In practice, some protein dissociation occurs on adding ADP and contributes directly to the observed fluorescence change. This can be quantitated either from the known actin-binding constant or by simultaneous light-scattering measurements (as shown in Fig. 4, *c* and *d*) and hence corrected for. For S1, there is only a small absolute change in light scattering on adding ADP, which is close to the

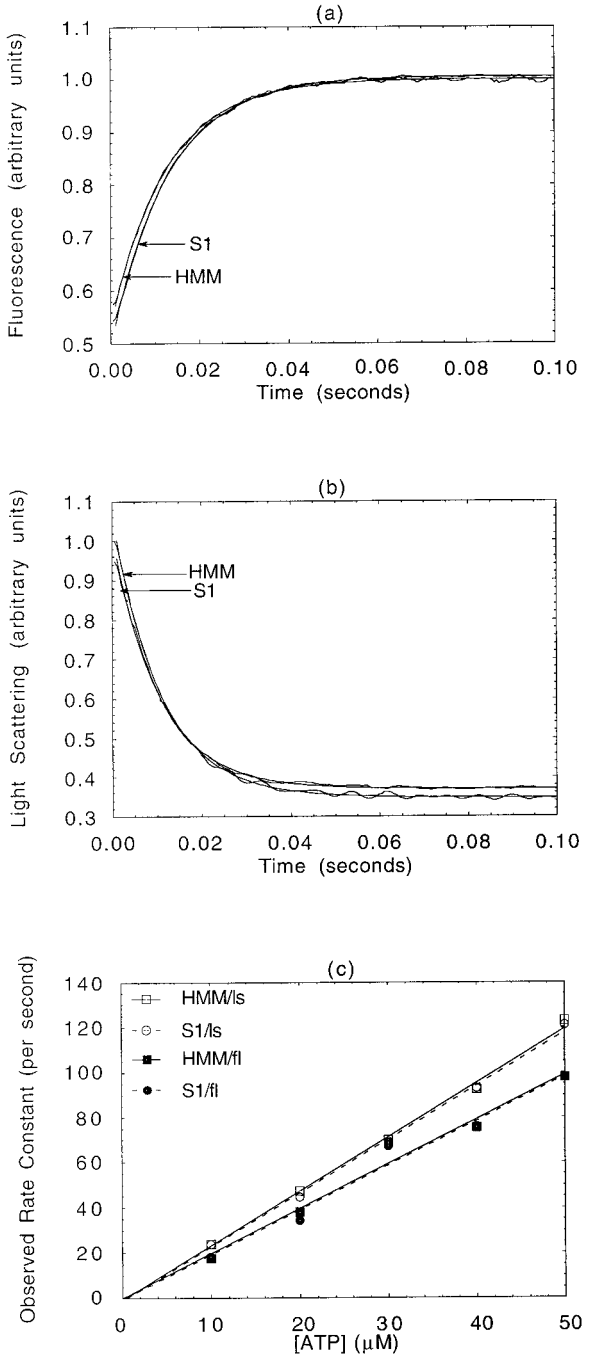

FIGURE 3 The dissociation of pyr-acto-S1 and pyr-acto-HMM upon rapid mixing with ATP in the stopped-flow apparatus. Transients are shown as monitored by both fluorescence (*a*) and light scattering (*b*) in successive pushes of the same samples. Chamber concentrations in this example are 2 μM acto-S1 (2 μM actin plus 2.2 μM S1) or 2 μM acto-HMM (2 μM actin plus 1.2 μM HMM) versus 40 μM ATP. Buffer conditions: 0.1 M KCl, 5 mM $MgCl_2$, 20 mM imidazole, pH 7.0, at 20°C. The transients shown are each averages of four raw transients and are unfiltered. They are shown fitted to single exponential functions (the brief lags not included) giving observed rate constants of: 76 s^{-1} (S1/fluorescence), 75.8 s^{-1} (HMM/fluorescence), 93 s^{-1} (S1/light scattering), and 92.4 s^{-1} (HMM/light scattering) and amplitudes (in the respective arbitrary units) of 0.51, 0.46, 0.64, and 0.72, respectively. (*c*) shows the dependence of the observed rate constant upon [ATP] yielding second-order rate constants (slopes) of 1.96×10^6 M^{-1} s^{-1}, 1.99×10^6 M^{-1} s^{-1}, 2.35×10^6 M^{-1} s^{-1}, and 2.39×10^6 M^{-1} s^{-1}, respectively. fl, fluorescence; ls, light scattering.

limits of the measurement. This reflects a lack of sensitivity owing to the large excess of S1 contributing a background signal. In this case, the fractional dissociation was better estimated from the measured value of K_S, which yielded a value of 3.2%. Thus, θ_S is estimated as 3.4%. This defines K_2 as 28.3. As $K_S = K_1(1 + K_2)$, then K_1 is defined as 2.3×10^4 M^{-1}, in agreement with earlier work (Geeves, 1989). For HMM, the light-scattering method is sufficiently sensitive and has the advantage of monitoring all actin subunits that dissociate whereas the measured value of K_H would yield an estimate corresponding only to the fraction of pairs of adjacent actins that had dissociated at the same time. The light-scattering measurements give a fractional dissociation of 7.2% (for individual actins). Thus, θ_H is 9%.

We have made measurements with at least four different preparations of both S1 and HMM (three purified by ion exchange chromatography and one by ammonium sulfate fractionation with the column purification step omitted). Differences between different preparations of the same protein were within the instrumental error with a consistent difference observed between HMM and S1. An additional experiment using HMM that had been subject to actin-affinity purification to remove nucleotide-resistant species also gave identical results. These findings suggest that minor contaminants with anomalous proteins present in variable amounts between different preparations do not account for the small differences observed between S1 and HMM. Rather, there is a small but genuine difference, reflecting the A-to-R transition for HMM compared with S1.

Analysis of cooperativity from equilibrium binding data

By summing contributions from each component state it can be shown that the following relationships hold for the proposed model (Fig. 1 *b*):

$$\frac{K_H}{4K_S} - 1 = \frac{K_1K_2C' + K_1K_2^2C'/x}{1 + K_2} \tag{7}$$

and

$$\theta_H = \frac{1 + K_1K_2C'}{1 + K_2 + 2K_1K_2C' + 2K_1K_2^2C'/x} \tag{8}$$

Using the measured values of K_S, K_1, K_2, K_H, and θ_H, we have calculated the values of C' and x by solution of these simultaneous equations. In addition, to test the model, we repeated the measurements for a range of conditions, over which the underlying values of K_S, K_1, and K_2 are independently modulated, and examined the covariation in the calculated values of C' and x. This is essentially a global fitting method, but the utility of the approach in this case lies in the fact that K_S, K_1, and K_2 can all be measured from experiments on S1 alone and are independent of the details of the cooperativity in HMM.

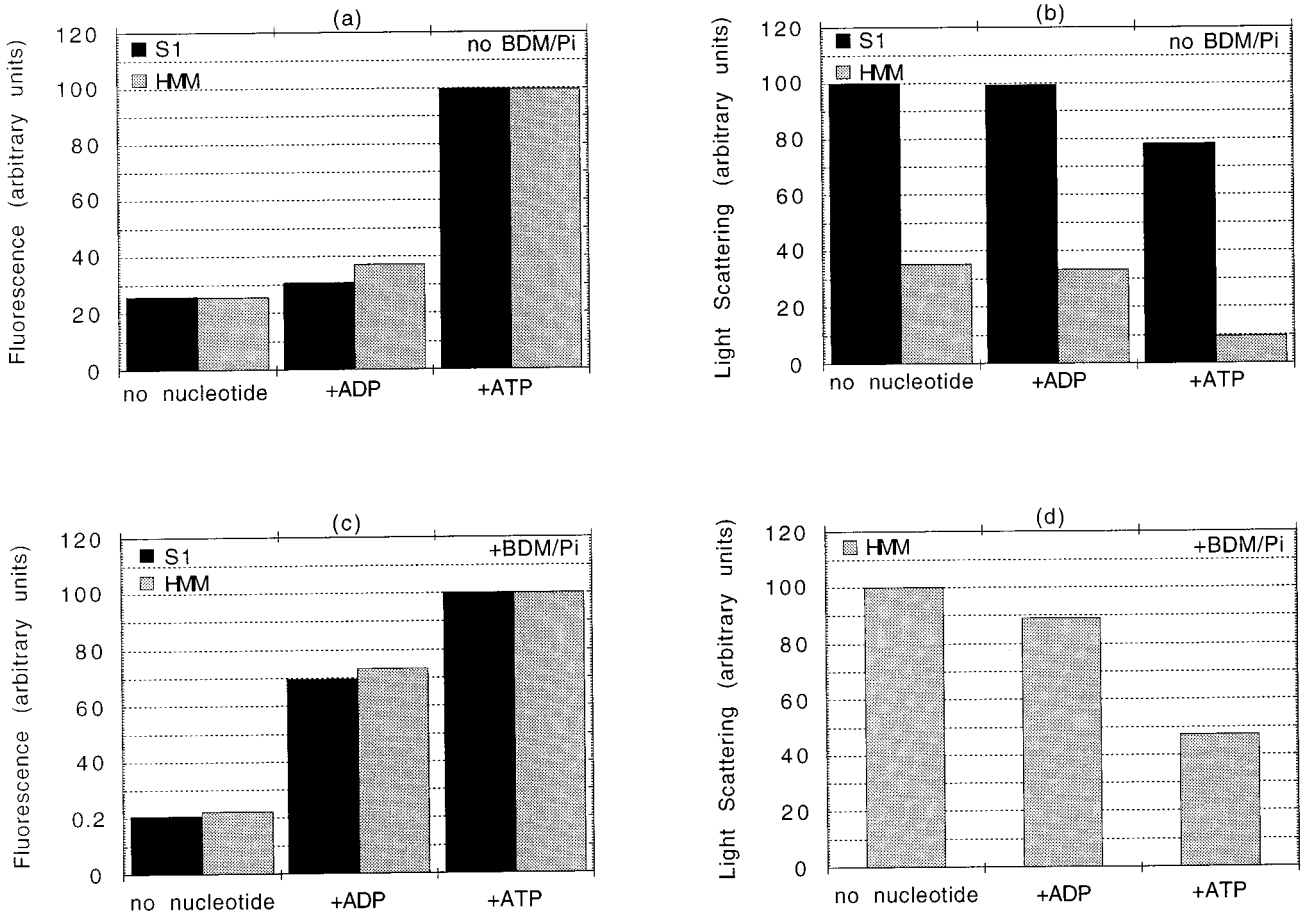

FIGURE 4 Measurement of θ_S and θ_H in the presence of ADP. Fluorescence (*a* and *c*) and light scattering (*b* and *d*) were measured in the fluorimeter for pyr-acto-S1 (*black bars*) and for pyr-acto-HMM (*gray bars*) in the absence of nucleotide (*left-hand bars*), after addition of 2 mM ADP (*middle bars*), and after the subsequent addition of 2 mM ATP (*right-hand bars*). Values are shown corrected for dilution (which was less than 5%). Buffer conditions: either 0.1 M KCl, 5 mM $MgCl_2$, 20 mM MOPS, pH 7.0, at 20°C (*a* and *b*) or 90 mM KPi, 5 mM $MgCl_2$, 20 mM BDM, pH 7.0, at 20°C (*c* and *d*). Protein concentrations are 5 μM actin and either 50 μM S1 or 7.5 μM HMM (*a* and *b*) and 5 μM actin and either 105 μM S1 or 7.5 μM HMM (*c* and *d*). No scattering measurements were made for S1 in the presence of BDM/Pi. The fraction of actin in the D- or A-state is determined from $(F_{ADP} - F_{NN})/(F_{ATP} - F_{NN})$ and is 6.5% and 61.6% (S1) and 15.4% and 65.5% (HMM) without and with BDM/Pi, respectively. For HMM, the fractional dissociation is determined from $(LS_{NN} - LS_{ADP})/(LS_{NN} - LS_{ATP})$ and is 7% and 20.9% without and with BDM/Pi, respectively. For S1, the fractional dissociation was estimated on the basis of the value of K_S measured by titration (in a buffer consisting of 2 mM ADP, 90 mM KPi, 5 mM $MgCl_2$, 20 mM BDM, pH 7.0, at 20°C, for BDM/Pi; see Table 1) yielding values of 3.2% and 9% without and with BDM/Pi, respectively. θ_S and θ_H are given in the table for the single data sets shown here (3.4%/9% without BDM/Pi and 57.8/56.4% with BDM/Pi, respectively). Extreme values for five other data sets with the same preparations are as follows: θ_S = 3.9%/2.9% and θ_H 9.1%/8.1% without BDM/Pi and θ_S = 59%/57.6% and θ_H = 57.1%/55% with BDM/Pi. This is within the random instrumental error.

Effects of ionic strength and Pi

For the analysis outlined above, we examined the effect of increased ionic strength (0.2 M KCl), which led to a twofold decrease in K_1 and a fourfold decrease in K_2, and in other experiments, we examined the combined effect of 2,3-butanedione 2-monoxime (BDM) and Pi (the latter was done exactly as for the preceding experiment but using a Pi buffer with 20 mM BDM present throughout; data for the latter are shown in Fig. 4). In our experiments, this led to the same overall decrease in K_S as the increase in ionic strength but with a 2.5-fold increase in K_1 and a larger (40-fold) decrease in K_2. BDM has previously been shown to result in a stabilization of the A-M · ADP · Pi state (McKillop et al., 1994). The earlier work suggests that Pi binding is unlikely to be saturated under the conditions used here, so the measured K_1 and K_2 values do not define the acto-S1 interaction for any particular nucleotide state. However, this is not a problem for our analysis because the quantitative behavior of our acto-HMM model is dependent upon the nucleotide bound only through its effect on the various actin-binding transitions.

Further variation of conditions was not useful because titration end-points become badly defined when the binding is weakened whereas the signal-to-noise ratio becomes untenable at the lower actin concentrations required when the binding is strengthened. More fundamentally, C' and x cannot be calculated with any accuracy under conditions where the second head does not bind significantly.

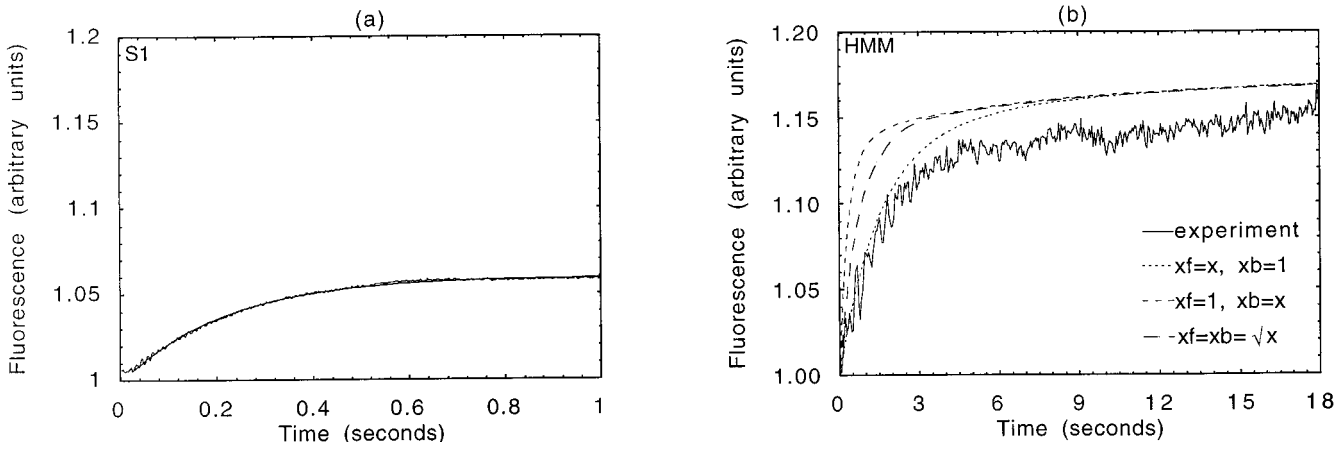

FIGURE 5 Fluorescence transients observed upon rapidly mixing either pyr-acto-S1 (*a*) or pyr-acto-HMM (*b*) with ADP in the stopped-flow apparatus. All transients shown are averages from at least three pushes, and both plates have a common vertical scale. Chamber concentrations were 1 μM actin plus 50 μM S1 (or 1 μM actin plus 1.5 μM HMM) versus 2 mM ADP. Buffer conditions were as for Fig. 4, but ADP was pretreated with hexokinase to eliminate contaminating ATP. ATP-induced dissociation was also measured in subsequent pushes and light-scattering transients were measured for both the ADP- and ATP-induced perturbations to determine C′ and x and for scaling of the simulated curves (see below). The S1 data are shown fitted to a single exponential, giving an observed rate constant of 4.7 s^{-1} (excluding a brief lag due to time constant of the amplifier). Simulations are shown for the HMM experiment with numerical values of fixed parameters set as follows: $k_{+1} = 4.7 \times 10^4$ M^{-1} s^{-1}; $k_{-1} = 1.74$ s^{-1}; $k_{+2} = 4.7$ s^{-1}; $k_{-2} = 0.2$ s^{-1}; $x = 7.06$ and $C' = 1.01 \times 10^{-4}$ M. For comparison with the experimental data, the simulated curves were scaled by the amplitude observed for ATP-induced dissociation and offset to the initial fluorescence. Both the experimental and simulated curves give an acceptable fit to the double exponential function $y = C + A_f(1 - \exp(-k_f t)) + A_s(1 - \exp(-k_s t))$. Fits are not shown but least-squares parameters are given in Table 2.

The measured and calculated parameters are summarized in Table 1 (the values are from single experiments, but the same column-purified preparation was used for each set of conditions). Within experimental error (both C' and x can be defined to within a factor of 2 in most cases), the calculated values are the same for all of the conditions used. The value of x cannot be accurately determined from the BDM/Pi experiments, as K_2/x is near zero. This, however, is consistent with a value of x close to those calculated from the other sets of experiments (the value in the table is to be regarded as a safe lower limit consistent with the values calculated in the absence of BDM/Pi). By this criterion, we conclude that the data fit the proposed model. On this model, C' is of the order of 100 μM, which corresponds closely to the local concentration of the tethered head estimated from the geometry. This suggests that when the first head is in the R-state, the second head can form the A-state (i.e., RD $\longleftrightarrow$ RA) unconstrained. The value of x is in the range 3.5–6.0, suggesting that the subsequent A-to-R transition (RA $\longleftrightarrow$ RR) can take place but with a reduced equilibrium constant compared with S1.

Dynamic studies

To examine the dynamics of the interaction with actin, we have monitored the ADP-induced fluorescence charge under the conditions of the experiment of Fig. 4 but by rapid mixing in the stopped-flow apparatus (Fig. 5). Also, we have examined the ADP association reaction itself using the competition between ADP binding and ATP-induced dissociation of the protein complex (White, 1977; data not shown). This showed that ADP binds rapidly and reversibly and that the affinity of both heads of HMM is identical to that of S1. Furthermore, both heads would be saturated with ADP within the dead time of the apparatus under the conditions of Fig. 5. The processes observed in Fig. 5 are therefore controlled not by ADP binding per se but by subsequent induced changes in the interaction between actin and the subfragments. For S1, a single exponential transient is observed at ~4 s^{-1}. This represents flux in part from A·M·ADP $\longleftrightarrow$ A-M·ADP without protein dissociation and in part from a dissociative process. The fact that only one phase is observed suggests that both contributory fluxes occur with similar rate constants (see below). For HMM, a biphasic transient is observed of which the fast phase is three- to fourfold slower than the process observed for S1.

Simulations

Because the model acto-HMM interaction is quite complex (i.e., more than two reversible steps), it is difficult to deduce

TABLE 1 Summary of the equilibrium binding data and analysis

Conditions	K_S (M^{-1})	K_1 (M^{-1})	K_2	K_H (M^{-1})	θ_S (%)	θ_H (%)	C' (μM)	x
ADP, 0.1 M KCl	6.7×10^5	2.3×10^4	28.4	3.3×10^7	3.4	9	89	6.1
ADP, 0.2 M KCl	1×10^5	1.2×10^4	7.1	1.5×10^6	12.3	16.1	87	3.6
ADP, BDM/Pi	1×10^5	5.8×10^4	0.73	1.5×10^6	57.8	56.4	124	≥4

TABLE 2 Least-squares parameters for Fig. 5

	k_f	k_s	A_f/A_s
Experiment	0.61	0.04	2.6
$x_f = x$, $x_b = 1$	0.67	0.12	2.7
$x_f = 1$, $x_b = x$	3.78	0.15	3.6
$x_f = x_b = x^{1/2}$	1.61	0.14	3.6

the rate constants analytically. To examine how the constraint upon the A-to-R transition is apportioned between the forward and backward rate constants, we simulated the transient by numerical integration based on the following kinetic scheme (essentially an ADP-binding step followed by the series of transitions in our working model for the acto-HMM interaction):

$$\{RR\} + 2ADP \rightleftharpoons RR \underset{k_{+2}/x_f}{\overset{k_{-2}x_b}{\rightleftharpoons}} RA \underset{k_{+1}C'}{\overset{k_{-1}}{\rightleftharpoons}} RD \underset{k_{+2}}{\overset{k_{-2}}{\rightleftharpoons}} AD \underset{4k_{+1}}{\overset{k_{-1}}{\rightleftharpoons}} DD + (Ac)_2 \quad (9)$$

In this terminology, k_{+n} and k_{-n} are the rate constants for the two-step binding of S1 to actin (such that $k_{+n}/k_{-n} = K_n$); x_f is the factor by which the forward rate constant of the specified A-to-R transition is reduced and x_b is the factor by which the backward rate constant is increased relative to that for S1 (so $x_f/x_b = x$). The fluorescence transient was simulated by computing the time course of (0.5*[RA] + 0.5*[RD] + [AD] + [$(Actin)_2$])/([RR] + [RA] + [RD] + [AD] + [$(Ac)_2$]). The values of x_f and x_b were covaried in successive runs keeping other parameters fixed at independently measured values. Pressure-relaxation measurements on acto-S1 (data not shown) were used to define k_{+1} and k_{-1} (Geeves, 1989). It was then possible to use the acto-S1 data of Fig. 5 *a* to define k_{+2} and k_{-2} (values used are given in the legend). These values are independent of any details of the acto-HMM interaction. C' and x were calculated using the method outlined above for analysis of the equilibrium data, but measurements were taken from the amplitudes of the transients in the present stopped-flow experiments rather from from the equilibrium data (although these are the same within instrumental error). In practice, the ADP-binding step was neglected because it is saturated, fast compared with the other steps, and complete in the dead-time, so that the bound complex at zero time was assumed to be in the RR-state (i.e., the ADP-bound state).

Note that none of the simulations provide a good match to the data over the slow phase. This phase appears to be controlled by events in which both heads become dissociated simultaneously and subsequently reassociate. Because of the limited number of free subunits on the filament, it is likely that a parking problem as described by Hill (1978) would have to be taken into account to simulate this part of the transient, and as such, the observed mismatch is not surprising. However, the fast phase appears to correspond to the preceding events before both heads dissociate and is not subject to such a problem. With respect to this fast phase, there is close correspondence when $x_f = x$ and $x_b = 1$. It is worse when $x_f = x_b = x^{1/2}$, although the simulations are still compatible with the data given the errors on the values used for C' and x. It is worse still when $x_f = 1$ and $x_b = x$ such that this latter case can be excluded. These data therefore require that the constraint upon the A-to-R transition occurs via a decrease in the forward (associative) rate constant. Modulation of backward (dissociative) rate constants is not required, although some effects cannot be excluded from this data alone. This is compatible with the finding that the ATP-induced dissociation kinetics are the same for both proteins (Fig. 3). As ATP-induced dissociation is controlled only by the backward rate constants, the data of Fig. 3 provide definitive evidence that these backward rate constants are unmodulated.

DISCUSSION

Given that our analysis is based on a particular model, it is important to consider the alternative models in which the binding is nonordered and nonpolar. Thus, using a similar type of analysis, we have tested other models based on the full scheme of Fig. 1 *a*, i.e., with all the possible states included (e.g., we assigned equilibrium constants on the basis that the second head has the same effective concentration for all actin-binding steps, C', and a reduction in the equilibrium constant by x-fold of all subsequent isomerizations). We have found that our equilibrium data can exclude models of this kind. Essentially, the form of the observed dependence of θ_H upon K_2 requires constraints upon at least two distinct steps with opposed effects on the overall equilibrium between A-states and R-states. Only the model proposed in the introduction fulfills this requirement as, on the one hand, the ordered/polar features tend to give an increased occupancy of the R-state for the first head, whereas, on the other hand, there is scope for a reduced occupancy of the R-state for the second head. We therefore conclude that this model is the simplest that can account for the data. Our analysis of the equilibrium data then suggest that there is little constraint upon RD $\longleftrightarrow$ RA ($C' = 100$ μM) but a clear constraint upon RA $\longleftrightarrow$ RR ($x = 4$–9) in addition to the constraints upon AA and AR inherent to our model. Our kinetic data indicate that the observed constraints operate only on the forward rate constants of the transitions. These conclusions come from kinetic modeling and as such are not dependent on any breakdown in the structural assumptions (e.g., stereospecificity of the A-state) made in proposing this model (the assumptions simply provided a rationale for considering this type of model a priori).

The lack of constraint upon the actin-binding step RD $\longleftrightarrow$ RA is compatible with the absence of both strain and orientation effects on this step, although it could in principle be the result of a fortuitous balance between the two effects. However, the observed constraint upon the subsequent isomerization RA $\longleftrightarrow$ RR provides definitive

evidence for an effect of steric strain and allows the effect to be quantitated (as, by definition, only actin-binding steps can be modulated by an orientation effect). The inhibition of the formation of AA and AR in our model is consistent with strain effects quantitatively similar to that operating on RA $\longleftrightarrow$ RR, but insufficient information is available from our data to define these effects more precisely.

Our approach has led to a more complex view of the nature of the cooperativity than has previously been acknowledged. This is essentially due to our ability to resolve cooperative effects on individual steps that are opposed and therefore cancel out in terms of the overall binding affinity; i.e., there are strain effects on both RA $\longleftrightarrow$ RR and on AD $\longleftrightarrow$ AA, both resulting in a weakening of the affinity, whereas, on the other hand, there is a strain effect on RR $\longleftrightarrow$ AR, which increases the affinity by a similar amount.

Structural models

The overall picture of steric strain that has emerged from our analysis is compatible with that depicted by the cartoon structures of Fig. 1. Furthermore, our experimental measure of the strain energy (associated with RA $\longleftrightarrow$ RR) is in reasonable quantitative agreement with that predicted from independently determined mechanical parameters: x can be calculated using $x^{-1} = \exp(-kl^2/2KT)$, where l is the working stroke, k is the stiffness of the elastic element in the myosin head, K is Boltzmann's constant, and T is the absolute temperature. Taking $l = 4$ nm (Molloy et al., 1995) and $k = 0.5$ pN nm^{-1} (Huxley and Simmons, 1971) leads to a value for x of 2.7. Only modest increases in the values assumed for either l or k are required to bring x to within the range calculated from our experimental data.

Implications for the ATPase cycle and contraction

It should be stressed that the discussion so far has related strictly to the cooperativity under dynamic equilibrium conditions. Perhaps more important from a functional point of view is the question of cooperativity during the active ATPase cycle. In the following paragraphs we consider this point. In doing so, we assume that the same constraints can potentially operate as in the dynamic equilibrium situation. We can consider three distinct modes of cycling: 1) in solubilized proteins, 2) in rapidly shortening muscle, and 3) in isometric muscle contraction.

Early work showed that under the low ionic strength conditions required to achieve maximal actin-activation of the ATPase, both the K_m (for actin) and the V_{max} are essentially the same (per head) for HMM compared with S1 (Eisenberg and Kielly, 1972). The same work suggested that under such conditions, a step in the detached phase of the pathway becomes rate limiting (Eisenberg and Kielly, 1972), now thought to be the hydrolysis step (Tesi et al., 1990). In this case, any given head spends only a small fraction of the cycle time attached to actin; i.e., the duty ratio is low (<0.2). Statistical considerations alone would then suggest that only one of the two heads binds to actin and cycles at any given time. This is consistent with the similar K_m values. The inability of the second head to bind does not affect the V_{max} value because this is controlled largely by hydrolysis. Oxygen exchange studies also showed that HMM and S1 are identical with regard to Pi-release kinetics, although at low ATP concentrations, differences were apparent due to the first head tethering the second head near the actin for the extended time required for the first head to bind ATP (Hackney and Clarke, 1984).

In rapidly shortening muscle, the cycle is less clearly understood but is probably analogous to that in solution at high actin activation. Whatever the details, the known shortening and ATPase rates are most easily reconciled by a low duty ratio (<0.03; Bagshaw, 1993). In this case, the conclusions regarding cooperativity are effectively the same as for the solution ATPase. In both situations, the additional constraints upon the binding of the second head that we have identified in the present work would have little operational consequence.

In isometric muscle, the cycle is different from either of the above modes in that the rate limitation is shifted to a slower step in the attached part of the cycle after formation of the R-state, possibly associated with ADP release (Goldman, 1987). In this case, the duty ratio is expected to be larger than during shortening and the binding of the second head may therefore become significant. In general, the binding of the second head might occur via a distinct actin filament (interfilament binding) as opposed to binding to an adjacent actin subunit on the same filament (intrafilament binding). The partitioning between these two modes of binding must be dependent on the actin concentration. At the relatively low actin concentrations used in solution, interfilament binding is unlikely to occur significantly, but at the higher concentrations in muscle it becomes more probable and has been observed at least in rigor (Taylor et al., 1984). However, little information on the nature of interfilament binding is available from our solution studies, and so we will consider only intrafilament binding in the following discussion.

The ordered binding mechanism identified in our work suggests that any binding of the second head would prevent the first head from reverting to the A-state during the final stages of its cycle. This may be an important factor for the generation of high tension in the isometric muscle. The constraints upon the second head isomerizing to the R-state would prevent this occurring during the cycle; i.e., any binding of the second head would be restricted to the A-state. The second head is not, however, expected to impose a constraint upon the ability of the first head to proceed into the next cycle via ATP-induced dissociation (given our finding that only associative rate constants are modulated). When the first head does dissociate, the constraints on the second head are hence removed. The subse-

quent fate of the second head depends on whether it is in the A-M·ADP·Pi or A-M·ADP states as these states show very different kinetics in solution (White and Taylor, 1976; Geeves, 1989). If, as is most likely, the second head is in the A-M·ADP·Pi state, it will dissociate rather than isomerizing to the R-state and proceeding through the cycle. If, however, it is in the A-M·ADP state, it will either dissociate or isomerize with roughly equal partitioning; i.e., neither event is obligatory.

Such a synchrony in the action of the two heads has been invoked in modeling studies (Davis and Rodgers, 1996; Huxley and Tideswell, 1997) to explain the mechanical responses of muscle fibers to rapid temperature jumps (Davis and Rodgers, 1995) and to rapid length steps (Lombardi et al., 1992), respectively. The findings of the present work might therefore represent a biochemical basis for these complex mechanical phenomena.

Processivity

An important characteristic of motor proteins is the degree of processivity. It is clear from numerous motility assays that skeletal muscle myosins are not processive (Howard, 1997). This would indeed follow from the fine details of the ATPase kinetics as discussed in the preceding paragraphs. However, it is striking that cooperativity of the kind we have identified provides a mechanism by which processivity could be achieved (i.e., the two heads are coordinated; the first head must isomerize to the R-state before the second binds in the A-state and the first head then undergoes unconstrained ATP-induced dissociation to allow the second head to proceed to the R-state). However, some fine tuning of the ATPase kinetics would be needed, too (specifically, shifting the rate-limiting step to an attached state transition and lowering actin dissociation rates via k_{-1}). Given the multitude of different myosins now identified and the potential for fine tuning (Mooseker and Cheney, 1995), it seems conceivable that such a mechanism might operate in other two-headed members of the myosin superfamily, most of which are yet to be characterized in detail with the possibility of processivity still open. Maybe the same mechanism operates in other processive motor proteins, too.

We thank Prof. H. Gutfreund for support and encouragement during this work, Dr. Neil Millar for providing us with the KSIM software, and Drs. David Smith and Sherwin Lehrer for critical reading of the manuscript.

This work was supported by the Royal Society (M.A. Geeves) and the Medical Research Council (Ph.D. studentship to P.B. Conibear). The experimental work was carried out at the Department of Biochemistry, University of Bristol. The work has been presented in preliminary form elsewhere (Conibear, 1993: Ph.D. thesis, University of Bristol, U.K.; Geeves and Conibear, 1995: Biophysical Society Discussions Meeting).

REFERENCES

Bagshaw, C. R. 1987. Are two heads better than one? *Nature*. 326: 746–747.

Bagshaw, C. R. 1993. Muscle Contraction, 2nd ed. Chapman and Hall, London.

Coates, J. H., A. H. Criddle, and M. A. Geeves. 1985. Pressure-relaxation studies of pyrene-labelled actin and myosin subfragment-1 from rabbit skeletal muscle. *Biochem. J.* 232:351–356.

Cooke, R. 1986. The mechanism of muscle contraction. *Crit. Rev. Biochem.* 21:53–118.

Criddle, A. H., M. A. Geeves, and T. Jeffries. 1985. The use of actin labelled with N-(1-pyrenyl)iodoacetamide to study the interaction of actin with myosin subfragments and troponin/tropomyosin. *Biochem. J.* 232:343–349.

Davis, J. S., and M. E. Rodgers. 1995. Force generation and temperature-jump and length-jump tension transients in muscle fibers. *Biophys. J.* 68:2032–2040.

Davis, J. S., and M. E. Rodgers. 1996. The two myosin heads function sequentially in non-tension and tension generating modes during isometric contraction. *Biophys. J.* 70:A126.

Eisenberg, E., and W. W. Kielly. 1972. Evidence for a refractory state of heavy meromyosin and subfragment-1 unable to bind to actin in the presence of ATP. *Cold Spring Harbor Symp. Quant. Biol.* 37:145–152.

Finlayson, B., R. W. Lymn, and E. W. Taylor. 1969. Studies on the kinetics of formation and dissociation of the actomyosin complex. *Biochemistry.* 8:811–819.

Geeves, M. A. 1989. Dynamic interaction between actin and myosin subfragment-1 in the presence of ADP. *Biochemistry*. 28:5864–5871.

Geeves, M. A. 1991. The dynamics of actin and myosin association and the crossbridge model of muscle contraction. *Biochem. J.* 274:1–14.

Geeves, M. A., and P. B. Conibear. 1995. The role of three-state docking of myosin subfragment-1 with actin in force generation. *Biophys. J.* 68:194s–201s.

Geeves, M. A., R. S. Goody, and H. Gutfreund. 1984. Kinetics of acto-S1 interaction as a guide to a model for the crossbridge cycle. *J. Muscle Res. Cell Motil.* 5:351–361.

Geeves, M. A., and T. Jeffries. 1988. The effect of nucleotide upon a specific isomerisation of actomyosin subfragment-1. *Biochem. J.* 256: 41–46.

Goldman, Y. E. 1987. Kinetics of the actomyosin ATPase in muscle fibres. *Annu. Rev. Physiol.* 49:637–654.

Goody, R. S., and K. C. Holmes. 1983. Crossbridges and the mechanism of muscle contraction. *Biochim. Biophys. Acta.* 726:13–39.

Greene, L. E. 1981. Comparison of the binding of heavy meromyosin and myosin subfragment-1 to F-actin. *Biochemistry*. 20:2120–2126.

Greene, L. E., and E. Eisenberg. 1980. The binding of heavy meromyosin to F-actin. *J. Biol. Chem.* 255:549–554.

Hackney, D. D., and P. K. Clarke. 1984. Catalytic consequences of oligomeric organization: kinetic evidence for tethered acto-heavy meromyosin at low ATP concentrations. *Proc. Natl. Acad. Sci. U.S.A.* 81: 5345–5348.

Hill, T. L. 1978. Binding of monovalent and divalent myosin subfragments onto sites on actin. *Nature.* 274:825–826

Hill, T. L., and E. Eisenberg. 1980. Theoretical consideration in the equilibrium binding of myosin fragments on F-actin. *Biophys. Chem.* 11:271–281.

Howard, J. 1997. Molecular motors: structural adaptations to cellular functions. *Nature*. 389:561–567.

Huxley, A. F., and R. M. Simmons. 1971. Proposed mechanism of force generation in striated muscle. *Nature*. 233:533–538.

Huxley, A. F., and S. Tideswell. 1997. Rapid regeneration of the power stroke in contracting muscle for attachment of second myosin head. *J. Muscle Res. Cell. Motil.* 18:111–114.

Kouyama, T., and K. Mihashi. 1981. Fluorimetry study of N-(1-pyrenyl)iodoacetamide-labelled F-actin. *Eur. J. Biochem.* 114:33–38.

Kron, S. J., Y. Y. Toyshima, T. Q. P. Uyeda, and J. A. Spudich. 1991. Assays for actin sliding movement over myosin-coated surfaces. *Methods Enzymol.* 196:399–416.

Kurzawa, S. E., and M. A. Geeves. 1996. A novel stopped-flow method for measuring the affinity of actin for myosin head fragments using μg quantities of protein. *J. Muscle Res. Cell. Motil.* 17:669–676.

Lehrer, S. S., and G. Kerwar. 1972. Intrinsic fluorescence of actin. *Biochemistry*. 11:1211–1217.

Lombardi, V., G. Piazzesi, and M. Linari. 1992. Rapid regeneration of the actin-myosin power stroke in contracting muscle. *Nature*. 355:638–641.

Margossian, S. S., and S. Lowey. 1982. Preparation of myosin and its subfragments from rabbit skeletal muscle. *Methods Enzymol.* 85:55–71.

McKillop, D. F. A., N. S. Fortune, K. W. Ranatunga, and M. A. Geeves. 1994. The influence of 2,3-butanedione 2-monoxime (BDM) on the interaction between actin and myosin in solution and in skinned muscle fibres. *J. Muscle Res. Cell Motil.* 15:309–318.

Miyata, M., T. Arata, and A. Inoue. 1989. Interaction of two heads of myosin with F-actin: binding of heavy meromyosin with F-actin in the absence of nucleotide. *J. Biochem (Tokyo)*. 105:103–109.

Molloy, J. E., J. E. Burns, J. Kendrick Jones, R. T. Tregear, and D. C. S. White. 1995. Movement and force produced by a single myosin head. *Nature*. 378:209–212.

Mooseker, M. S., and R. E. Cheney. 1995. Unconventional myosins. *Annu. Rev. Cell Dev. Biol.* 11:633–675.

Offer, G., and A. Elliott. 1978. Can a myosin molecule bind to two actin filaments? *Nature*. 271:325–329.

Rayment, I., H. M. Holden, M. Whittaker, C. B. Yohn, M. Lorenz, K. C. Holmes, and R. A. Milligan. 1993. Structure of the actin-myosin complex and its implications for muscle contraction. *Science*. 261:58–65.

Taylor, E. W. 1979. Mechanism of actomyosin ATPase and the problem of muscle contraction. *Crit. Rev. Biochem.* 6:103–164.

Taylor, K. A., M. C. Reedy, L. Cordova, and M. K. Reedy. 1984. Three-dimensional reconstruction of rigor insect flight muscle from tilted thin sections. *Nature*. 310:285–291.

Tesi, C., T. Barman, and F. Travers. 1990. Is a four-state model sufficient to describe the actomyosin ATPase. *FEBS Lett.* 260:229–232.

White, H. D. 1977. Magnesium-ADP binding to acto-myosin subfragment-1 and acto-heavy meromyosin. *Biophys. J.* 17:A40.

White, H. D., and E. W. Taylor. 1976. Energetics and mechanism of actomyosin adenosine triphosphatase. *Biochemistry*. 15:5818–5826.